Inorganic Chemistry

Article

pubs.acs.org/IC

Quasi-Three-Coordinate Iron and Cobalt Terphenoxide Complexes $\{Ar^{iPr_8}OM(\mu\text{-}O)\}_2$ (Ar^{iPr_8} = C_6H-2,6-(C_6H_2-2,4,6-$^iPr_3$)$_2$-3,5-$^iPr_2$; M = Fe or Co) with $M(III)_2(\mu\text{-}O)_2$ Core Structures and the Peroxide Dimer of 2-Oxepinoxy Relevant to Benzene Oxidation

Pei Zhao,[†] Hao Lei,[†] Chengbao Ni,[†] Jing-Dong Guo,[‡] Saeed Kamali,[†,∥] James C. Fettinger,[†] Fernande Grandjean,[§] Gary J. Long,*[,§] Shigeru Nagase,*[,‡] and Philip P. Power*[,†]

[†]Department of Chemistry, University of California, Davis, California 95616, United States

[‡]Fukui Institute for Fundamental Chemistry, Kyoto University, Takano-Nishihiraki-cho, Sakyo-ku, Kyoto 606-8103, Japan

[§]Department of Chemistry, Missouri University of Science and Technology, University of Missouri, Rolla, Missouri 65409-0010, United States

Supporting Information

ABSTRACT: The bis(μ-oxo) dimeric complexes $\{Ar^{iPr_8}OM(\mu\text{-}O)\}_2$ (Ar^{iPr_8} = C_6H-2,6-(C_6H_2-2,4,6-$^iPr_3$)$_2$-3,5-$^iPr_2$; M = Fe (**1**), Co (**2**)) were prepared by oxidation of the M(I) half-sandwich complexes $\{Ar^{iPr_8}M(\eta^6\text{-arene})\}$ (arene = benzene or toluene). Iron species **1** was prepared by reacting $\{Ar^{iPr_8}Fe(\eta^6\text{-benzene})\}$ with N_2O or O_2, and cobalt species **2** was prepared by reacting $\{Ar^{iPr_8}Co(\eta^6\text{-toluene})\}$ with O_2. Both **1** and **2** were characterized by X-ray crystallography, UV−vis spectroscopy, magnetic measurements, and, in the case of **1**, Mössbauer spectroscopy. The solid-state structures of both compounds reveal unique $M_2(\mu\text{-}O)_2$ (M = Fe (**1**), Co(**2**)) cores with formally three-coordinate metal ions. The Fe···Fe separation in **1** bears a resemblance to that in the $Fe_2(\mu\text{-}O)_2$ diamond core proposed for the methane monooxygenase intermediate *Q*. The structural differences between **1** and **2** are reflected in rather differing magnetic behavior. Compound **2** is thermally unstable, and its decomposition at room temperature resulted in the oxidation of the Ar^{iPr_8} ligand via oxygen insertion and addition to the central aryl ring of the terphenyl ligand to produce the 5,5′-peroxy-bis[4,6-$^iPr_2$-3,7-bis(2,4,6-$^iPr_3$-phenyl)oxepin-2(5*H*)-one] (**3**). The structure of the oxidized terphenyl species is closely related to that of a key intermediate proposed for the oxidation of benzene.

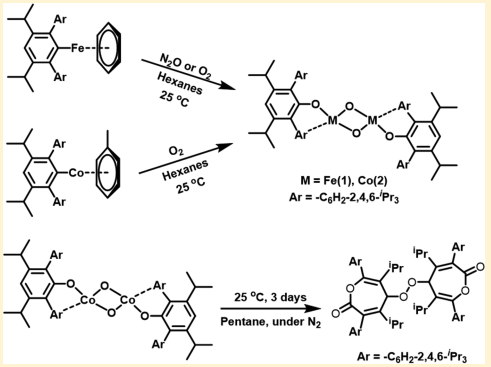

INTRODUCTION

Metal-mediated oxidation of C−H bonds is of fundamental importance in organic synthesis, industrial catalytic processes, and enzymatic reactions.[1−9] For the latter, methane monooxygenase (MMO), which catalyzes the oxidation of methane to methanol, has been proposed featuring a high-valent $Fe_2(\mu\text{-}O)_2$ diamond core structure as the key oxidizing species in the proposed mechanism of the catalytic cycle.[10−16] A number of synthetic complexes featuring $Fe_2(\mu\text{-}O)_2$ diamond cores with six-coordinate iron and Fe···Fe distances in the range 2.6−2.8 Å have been structurally characterized.[17−21] A recently reported complex $[\{(N,N'\text{-Pipiso})Fe(\mu\text{-}O)\}_2]$ (Pipiso$^-$ = [(DippN)$_2$C-(*cis*-2,6-$Me_2NC_5H_8$)]$^-$, Dipp = $C_6H_3Pr^i_2$-2,6) containing a bis(μ-oxo)diiron(III) core structure has a relatively short Fe···Fe distance (2.475(1) Å) with four-coordinate iron ions.[22]

A few bis(μ-oxo)dicobalt(III) complexes are also known. In 1998, Hikichi and co-workers reported[23,24] and structurally characterized the bis(μ-oxo)dicobalt(III) complex, which was stabilized by hydrotris(pyrazolyl)borate ligand. Since then, three other types of complexes containing a $Co_2(\mu\text{-}O)_2$ core $[Co^{III}H_2L(\mu\text{-}O)]_2^{2-}$ anion (H_2L = bis[(*tert*-butyl)-aminocarbonyl]-1,2-diamidoethane), $\{[Me_2NN]Co\}_2(\mu\text{-}O)_2$ (Me_2NN^- = $[HC\{C(Me)NC_6H_3$-2,6-$Me_2\}_2]^-$), and [{(priso)-Co(μ-O)}$_2$] (priso$^-$ = $[(ArN)_2CNiPr_2]^-$; Ar = 2,6-diisopropylphenyl) were reported by different groups through different synthetic routes.[25−27]

In our investigations of the reactivity of terphenyl-stabilized half-sandwich complexes, $\{Ar^{iPr_8}M(\eta^6\text{-arene})\}$ (Ar^{iPr_8} = C_6H-2,6-(C_6H_2-2,4,6-$^iPr_3$)$_2$-3,5-$^iPr_2$; M = Fe[28] or Co;[29] arene = benzene or toluene), we have found that they can act as starting materials for the synthesis of related high-valent metal complexes. For instance, the Fe(I) complex $\{Ar^{iPr_8}Fe(\eta^6\text{-}C_6H_6)\}$ reacts with 2 equiv of 1-adamantyl azide to afford an unusual Fe(V) bis(imido) compound, $[Ar^{iPr_8}Fe\{N(1\text{-Ad})\}_2]$.[30] Now we report that the oxidation of $\{Ar^{iPr_8}M(\eta^6\text{-arene})\}$ with N_2O or O_2 gives the dinuclear M(III) bis(μ-oxo) complexes, $\{Ar^{iPr_8}OM(\mu\text{-}O)\}_2$ (M = Fe (**1**), Co (**2**)), in which the metal

Received: April 24, 2015
Published: September 2, 2015

DOI: 10.1021/acs.inorgchem.5b00930
Inorg. Chem. 2015, 54, 8914−8922

ions are formally three-coordinate. In complex **1**, the Fe···Fe distance is 2.4817(7) Å, and approaches the value observed (2.46 Å) in the MMO intermediate *Q*. Complex **2** is thermally unstable and decomposes to give a number of products, one of which is 5,5′-peroxy-bis[4,6-^{i}Pr$_2$-3,7-bis(2,4,6-^{i}Pr$_3$-phenyl)-oxepin-2(5*H*)-one] (**3**) in which an oxygen atom is both inserted into and added to an aryl ring. The oxygen insertion into the aryl ring of an aryloxide ligand has also been observed in the nonheme iron containing enzyme homoprotocatechuate 2,3-dioxygenase (HPCD).[31−33] The isolation of the structure of **3** provides strong support for a key intermediate proposed for the oxidation of benzene, an important reaction in fuel autoignition[34] and atmospheric chemistry.[35−37]

EXPERIMENTAL SECTION

General Procedures. All operations were carried out by using modified Schlenk techniques under an atmosphere of dry argon or nitrogen. Solvents were dried over an alumina column and degassed prior to use. The starting materials, {Ar^{iPr_8}M(η^6-arene)} (Ar^{iPr_8} = C$_6$H-2,6-(C$_6$H$_2$-2,4,6-^{i}Pr$_3$)$_2$-3,5-^{i}Pr$_2$; M = Fe[28] or Co;[29] arene = benzene or toluene), were prepared according to literature procedures.[28,29] High-purity (>99.99%) N_2O and O_2 were dried through a P_2O_5 column prior to use. IR spectra were recorded as Nujol mulls between CsI plates on a Perkin-Elmer 1430 ratio recording infrared spectrometer. UV−vis spectra were recorded on a Hitachi-1200 spectrometer. NMR spectra were recorded on a Varian VNMRS 600 MHz spectrometer.

Synthesis of {Ar^{iPr_8}OFe(μ-O)}$_2$ (1). Method A. An orange solution of {Ar^{iPr_8}Fe(η^6-C$_6$H$_6$)} (0.30 g, 0.43 mmol) in ca. 30 mL of hexanes was treated with dry N_2O gas (1 atm). The mixture was exposed to the N_2O atmosphere for ca. 2 h and then sealed and stirred overnight at room temperature, by which time the solution had become a deep red color. The solution was filtered and concentrated to ca. 5 mL to afford X-ray quality deep red crystals of **1**·2.5C$_6$H$_{14}$ after storage for 1 day at −30 °C. Yield: 0.23 g (82%). Mp: 193 °C. ^{1}H NMR (600 MHz, C$_6$D$_6$, 24 °C): δ 7.29 (s), 7.27 (s), 7.02 (s), 7.00 (s), 3.27 (s), 2.99 (s), 2.34 (br), 1.91 (br), 1.46 (br), 1.31−1.23 (m), 1.15−1.12 (m), 0.97−0.95 (m), 0.90−0.88 (m), 0.85−0.80 (m), 0.27 (d), 0.18−0.14 (m), −0.533 (br). UV−vis [hexanes; λ_{max}, nm (ε, L mol^{-1} cm^{-1})]: 312 (17 200), 488 (5600).

Synthesis of {Ar^{iPr_8}OFe(μ-O)}$_2$ (1). Method B. An orange solution of {Ar^{iPr_8}Fe(η^6-C$_6$H$_6$)} (0.44 g, 0.63 mmol) in ca. 30 mL of hexanes was treated with dry O_2 gas (1 atm). The mixture was exposed to the O_2 atmosphere for ca. 30 min. The solution immediately became a deep red color. The flask was sealed and stirred for another 30 min at room temperature. The solution was filtered and concentrated to ca. 5 mL to afford deep red crystals of **1**·2.5C$_6$H$_{14}$ after storage for 1 day at −18 °C. Yield: 0.31g (65%).

Synthesis of {Ar^{iPr_8}OCo(μ-O)}$_2$ (2). A green solution of {Ar^{iPr_8}Co(η^6-C$_7$H$_8$)} (1.42 g, 1.98 mmol) in ca. 30 mL of hexanes was treated with dry O_2 gas (1 atm) at room temperature for 30 min. The solution immediately became deep blue-green, and after stirring for 1 h, the solution was concentrated to ca. 5 mL, which upon storage at −30 °C for 2 weeks afforded X-ray quality deep blue-green crystals of **2**·2.5C$_6$H$_{14}$. Yield: 0.49 g (38%). Mp: 187 °C (decomp). ^{1}H NMR (600 MHz, C$_6$D$_6$, 24 °C): δ 11.66 (s), 10.38 (d), 10.10 (s), 9.96 (s), 9.44 (s), 7.69 (s), 7.54 (s), 7.34 (s), 7.23 (s), 7.03 (s), 6.96 (s), 6.88 (s), 6.66 (s), 4.39 (s), 3.70 (br), 2.90−2.59 (m), 1.97 (br), 1.29−1.09 (m), 0.89−0.84 (m), −0.72 (s). UV−vis [hexanes; λ_{max}, nm (ε, L mol^{-1} cm^{-1})]: 232 (49 000), 284 (31 000), 708 (9800).

Decomposition of 2 to 5,5′-Peroxy-bis[4,6-^{i}Pr$_2$-3,7-bis(2,4,6-^{i}Pr$_3$-phenyl)oxepin-2(5H)-one] (3). A deep blue-green solution of **2** (0.56 g, 0.43 mmol) in ca. 30 mL of pentane was sealed under nitrogen gas and stirred for 3 days, by which time the color of the solution gradually changed to orange-brown. The solution was filtered and then concentrated to ca. 2 mL, which upon storage at ca. −30 °C for 2 weeks afforded colorless crystals of **3** suitable for X-ray diffraction. Yield: 30 mg (6%). HRMS *m*/*z* calculated for C$_{84}$H$_{122}$O$_6$ [M$^+$] 1226.9241, found 1226.9491; calcd for C$_{42}$H$_{61}$O$_3$ [M$^+$] 613.4621, found 613.4622. IR v/cm^{-1} (Nujol): 1450s, 1370s, 1260s, 1010s, 910s, 800s, 720s.

Magnetic Measurements. The samples for magnetic measurements were sealed under vacuum in 4 mm diameter quartz tubes. The magnetic properties were measured on a Quantum Design MPMSXL7 SQUID magnetometer. The sample was initially zero-field cooled to 2 K, and the magnetic susceptibility was then measured from 2 to 300 K in a 0.010 T applied magnetic field over a period of approximately 14 h. The observed molar magnetic susceptibilities have been corrected for the diamagnetic contribution of the constituents by subtracting −0.001 089 and −0.000 895 emu/mol for **1** and **2**, respectively, values that have been obtained from tables of Pascal's constants.[38]

Mössbauer Spectroscopy. The 80 K spectrum was measured using a Janis SVT-400 cryostat with a MS4 spectrometer operating in constant acceleration mode with a room temperature 100 mCi ^{57}Co in Rh source. All isomer shifts, δ's, are given relative to room-temperature α-iron. The errors associated with the spectral parameters reported below are the statistical errors; the actual errors are most likely 2−3 times larger.

X-ray Crystallographic Studies of 1·2.5C$_6$H$_{14}$, 2·2.5C$_6$H$_{14}$, and 3. Crystals suitable for X-ray diffraction studies were removed from a Schlenk tube under a stream of nitrogen and immediately covered with a thin layer of hydrocarbon oil. A suitable crystal was selected, attached to a glass fiber on a copper pin, and quickly placed in the cold N_2 stream on the diffractometer. Data for compounds **1** and **2** were collected at 90 K on a Bruker SMART APEX II diffractometer with 0.710 73 Å Mo Kα radiation. Compound **3** was collected at 90 K with 1.5418 Å Cu Kα_1 radiation on a Bruker DUO-APEX-II diffractometer in conjunction with a CCD detector. Absorption corrections were applied using SADABS.[39] The crystal structures were solved by direct methods and refined by full-matrix least-squares procedures with SHELXTL.[40] All non-H atoms were refined anisotropically. All H atoms were placed at calculated positions and included in the refinement by using a riding model. Data collection parameters are summarized in Table S1 (Supporting Information).

Density Functional Calculations. All calculations were carried out by using the Gaussian 09 program.[41] Geometry optimization was performed with hybrid density functional theory (DFT) at the M06-2x level, by using the 6-311+G(d) basis set for the iron and cobalt cations, the 6-31G(d) basis set for oxygen, and the 6-31G basis set for C and H atoms. The UV−vis absorption spectra of optimized geometries were calculated with the time dependent (TD) DFT method at the CAM-B3LYP[42] level containing long-range correlation for **1** and B3LYP level for **2**.

Electrochemistry. Electrochemical measurements were recorded in a glovebox under a N_2 atmosphere using a CH Instruments Electrochemical Analyzer, a glassy-carbon working electrode, a platinum-wire auxiliary electrode, and an Ag/AgNO$_3$ nonaqueous reference electrode. All experiments were performed under a N_2 atmosphere with 0.1 M Bu$^n_4$NPF$_6$ in THF as the electrolyte. Compound **1** was measured at room temperature. Compound **2** was measured at −78 °C due to the instability of the compound.

RESULTS AND DISCUSSION

Synthesis. {Ar^{iPr_8}Fe(η^6-C$_6$H$_6$)}[28] reacted smoothly with N_2O at 1 atm to afford a dark red solution upon stirring overnight. The unique dimeric iron(III) complex, {Ar^{iPr_8}OFe(μ-O)}$_2$ (**1**) (see below, Figure 1), was isolated from a hexanes solution as deep red crystals in high yield (Scheme 1) by cooling to ca. −30 °C. We found that **1** was also obtained by the exposure of a hexanes solution of {Ar^{iPr_8}Fe(η^6-C$_6$H$_6$)} to dry O_2 for 30 min. An overnight reaction of {Ar^{iPr_8}Fe(η^6-C$_6$H$_6$)} with dry O_2 led to intractable brown mixtures from which no crystalline products could be obtained. In contrast, the cobalt analogue, {Ar^{iPr_8}Co(η^6-C$_7$H$_8$)}, did not react with N_2O, even at elevated temperature. However, exposure of {Ar^{iPr_8}Co(η^6-C$_7$H$_8$)} to a large excess of O_2 at 1 atm resulted in an immediate color change from bright green to a deep blue-

DOI: 10.1021/acs.inorgchem.5b00930
Inorg. Chem. 2015, 54, 8914−8922

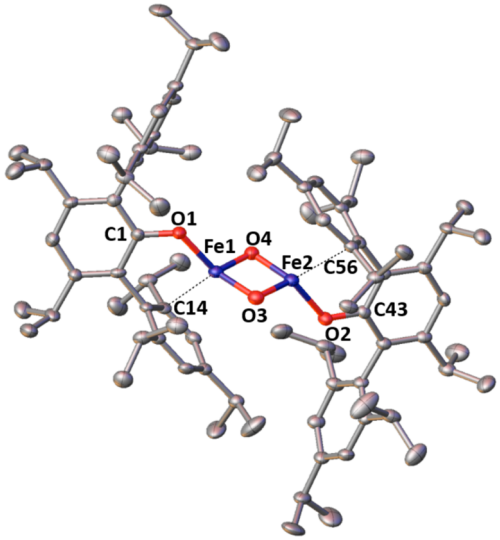

Figure 1. Solid-state molecular structure of **1** (H atoms and solvent molecules are not shown, thermal ellipsoids are shown at 50% probability). Selected bond lengths (Å) and angles (deg): Fe(1)···Fe(2) 2.4817(7), Fe(1)−O(1) 1.864(2), Fe(2)−O(2) 1.874(2), Fe(1)−O(3) 1.818(3), Fe(1)−O(4) 1.824(2), Fe(2)−O(3) 1.829(2), Fe(2)−O(4) 1.816(2), Fe(1)···C(14) 2.457(3), Fe(2)···C(56) 2.427(3), O(3)−Fe(1)−O(4) 94.17(11), O(1)−Fe(1)−O(3) 124.19(11), O(1)−Fe(1)−O(4) 116.16(1), Fe(1)−O(4)−Fe(2) 85.99(11), O(3)−Fe(2)−O(4) 94.06(11), O(2)−Fe(2)−O(3) 119.7(1), O(2)−Fe(2)−O(4) 119.13(11), Fe(2)−O(3)−Fe(1) 85.76(11), Fe(1)−O(1)−C(1) 127.2(2), Fe(2)−O(2)−C(43) 126.4(2).

Scheme 1. Synthetic Routes for 1 and 2

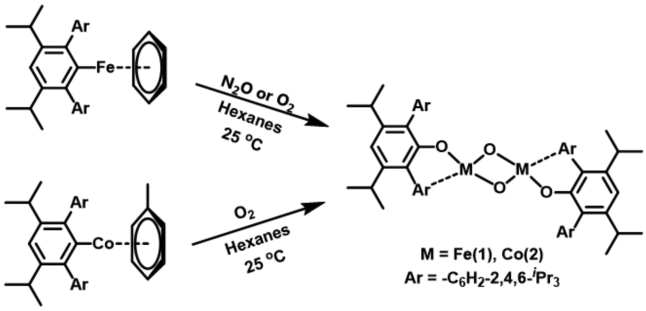

green and gave, after recrystallization from hexanes, deep blue-green crystals of $\{Ar^{iPr_8}OCo(\mu\text{-}O)\}_2$ (**2**) (see below, Figure 2) in moderate yield. Thus, the synthesis of both **1** and **2** involves a two electron oxidation of the metal and the addition of two oxygens per metal, one of which is inserted into a metal−carbon σ-bond. The oxidation may be contrasted with that of the Fe(II) diaryl $Fe(Ar^{iPr_4})_2$ (Ar^{iPr_4} = C_6H_3-2,6-(C_6H_3-2,6-$^i Pr_2$)$_2$), which afforded $Fe(OAr^{iPr_4})_2$ via the reaction of $Fe(Ar^{iPr_4})_2$ and O_2. The reaction does not result in the oxidation of the iron but is limited to the insertion of oxygen into the Fe−C bond.[43] DFT studies based on the model system $FeMe_2 + O_2 \rightarrow Fe(OMe)_2$ have provided support for a reaction pathway with O_2 that involves a sequence of Fe^{III}-superoxo, Fe^{VI}-dioxo, and Fe^{IV}-oxo intermediates.[44] On the basis of these results, we propose that the formation of **1** with dioxygen as the oxidant may follow a route similar to that calculated in ref 44: a superoxo species $Ar^{iPr_8}Fe(II)(O_2)$ may be formed initially by coordination of a dioxygen molecule to the Fe(I) center, and then the O−O scission could occur to give a dioxo Fe(V) intermediate $Ar^{iPr_8}Fe(V)(O)_2$. This is followed by the ligand migration/oxo-insertion to give $Ar^{iPr_8}OFe(III)(O)$; the $Ar^{iPr_8}OFe(III)(O)$ species dimerizes to give the final product **1**. It is also possible that the dioxo Fe(V) intermediate is formed through a dinuclear pathway as was shown in the reaction between a Cr(I) complex and O_2.[45] In this case 2 equiv of the Fe(I) starting material reacts with 1 equiv of O_2 to generate a dinuclear Fe(III) bis(μ-oxo) intermediate, namely, $[Ar^{iPr_8}Fe(\mu\text{-}O)]_2$, followed by reaction with another equivalent of O_2 to induce the dissociation of the dinuclear species $[Ar^{iPr_8}Fe(\mu\text{-}O)]_2$ and the formation of 2 equiv of the aforementioned dioxo Fe(V) intermediate $Ar^{iPr_8}Fe(V)(O)_2$. After the dioxo Fe(V) intermediate is formed, it is followed by the ligand migration/oxo-insertion to form $Ar^{iPr_8}OFe(III)(O)$ and the dimerization of $Ar^{iPr_8}OFe(III)(O)$ to give **1**.

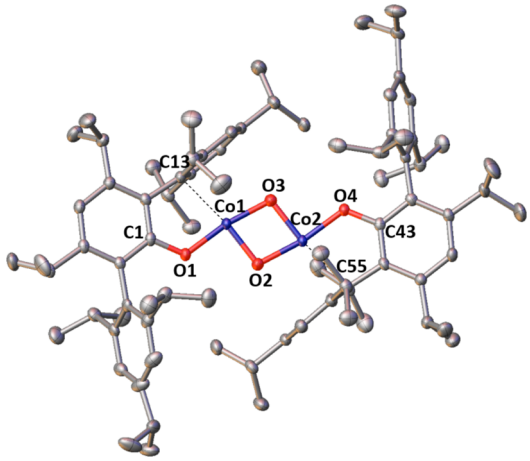

Figure 2. Solid-state molecular structure of **2** (H atoms and solvent molecules are not shown, thermal ellipsoids are shown at 50% probability). Selected bond lengths (Å) and angles (deg): Co(1)···Co(2) 2.7209(4), Co(1)−O(1) 1.8287(13), Co(1)−O(2) 1.7777(13), Co(1)−O(3) 1.7690(14), Co(2)−O(2) 1.7737(14), Co(2)−O(3) 1.7831(14), Co(2)−O(4) 1.8299(13), Co(1)···C(13) 2.2867(18), Co(2)···C(55) 2.2672(18), O(1)−Co(1)−O(2) 91.16(7), O(2)−Co(1)−O(3) 80.13(6), O(1)−Co(1)−O(3) 189.21(8), O(2)−Co(2)−O(3) 79.86(6), O(2)−Co(2)−O(4) 189.00(7), O(3)−Co(2)−O(4) 91.61(7), Co(1)−O(3)−Co(2) 99.99(7), Co(2)−O(2)−Co(1) 100.02(7), C(1)−O(1)−Co(1) 120.48(12), C(43)−O(4)−Co(2) 120.51(12).

Although the yield of **1** is high, the relatively lower isolated yield for **2** is probably due to the combination of its very high solubility in common organic solvents as well as the relatively low stability of the compound at ambient temperature which leads to its decomposition upon storage at room temperature either under a nitrogen atmosphere or in a vacuum. This is consistent with the observation that bis(μ-oxo)dimetal cationic cores for the later transition metal cations (Fe−Cu) tend to be rather reactive and unstable at room temperature.[17] Both **1** (488 nm, ε = 5600 L mol^{-1} cm^{-1}) and **2** (708 nm, ε = 9800 L mol^{-1} cm^{-1}) feature intense absorptions in their electronic spectra, which are probably a result of ligand to metal cation charge-transfer transitions. The mechanism whereby **2** is formed is probably similar to that of the formation of **1**.

The decomposition product **3** was isolated by allowing a pentane solution of **2** to stand at room temperature under a nitrogen atmosphere for 3 days. The solution color gradually changed from a deep blue-green color to orange-brown. Colorless crystals of 5,5′-peroxy-bis[4,6-$^i Pr_2$-3,7-bis(2,4,6-$^i Pr_3$-phenyl)oxepin-2(5*H*)-one] (**3**) were isolated from this solution

DOI: 10.1021/acs.inorgchem.5b00930
Inorg. Chem. 2015, 54, 8914−8922

in low yield (Scheme 2). The reactions of many late transition metal-oxo species with hydrocarbons afford either C−H bond

Scheme 2. Decomposition of 2 to 5,5′-Peroxy-bis[4,6-$^{i}Pr_2$-3,7-bis(2,4,6-$^{i}Pr_3$-phenyl)oxepin-2(5*H*)-one] (3)

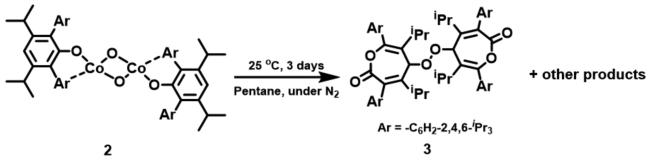

oxidation or oxygen atom transfer, such as sulfoxidation or epoxidation.[5−9] However, in the decomposition of **2**, oxidation of the C−C bond has occurred, and a peroxy moiety is finally formed. The formation of **3** probably occurs through a radical mechanism. The X-band EPR spectroscopy of **2** afforded a very narrow signal at $g \approx 2$, which is characteristic for main group element centered radicals but not for unpaired electrons that are centered on cobalt ions. Radical mechanisms have often been proposed for transition metal-oxo mediated reactions,[5−9,46] and it is noteworthy that an oxidized product resembling **3** was proposed as one of the key intermediates in the oxidation of benzene via oxygen initiated decomposition of a 2-oxepinoxy radical (Scheme 3): a phenyl radical reacts with

Scheme 3. Computational Study of the Generation of 2-Oxepinoxy Radical and Oxygen Initiated Decomposition of 2-Oxepinoxy Radical During the Oxidation of Benzene[47]

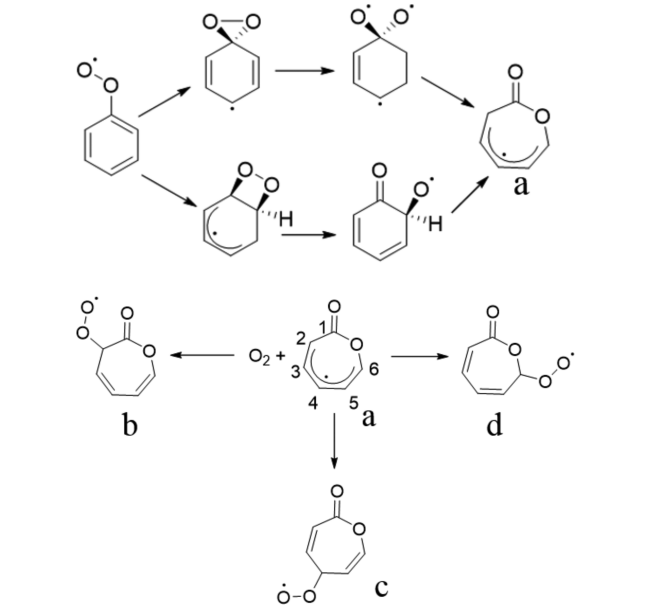

molecular oxygen to form a phenylperoxy radical, which then rearranges to a 2-oxepinoxy radical (a). The 2-oxepinoxy radical reacts further with an oxygen molecule to form three isomers of peroxyoxepinone radical (b−d).[47,48] For **2** it is possible that the cobalt-bis(μ-oxo) diamond core forms a cobalt-oxyl radical species to initiate the autoxidation, which was also proposed previously by Hikichi and Akita.[24] Subsequently the aryloxide ligand is attacked by the cobalt-oxyl species to form an arylperoxy radical, which then rearranges to the oxepinoxy species, followed by the attack of another cobalt-oxy radical to form an oxyoxepinone radical. This oxyoxepinone radical species may then couple with another oxyoxepinone radical to form **3**. It is noteworthy that only the 4-ring-carbon position is peroxidized, due to the fact that the 2-, 3-, 5- and 6-central ring carbon positions have aryl or isopropyl group substituents. However, it should be borne in mind that the actual details of the proposed mechanism have not been substantiated by experiment. A decomposition product containing cobalt(II) was also isolated from the mixture by fractional crystallization as orange crystals. A partial structure (Figure S1) shows that it has a framework similar to that of **2** except that the bridging oxygens have become bonded to a flanking aryl ring from one of the OAr^{iPr_8} ligands. This structure supports the radical character and reactivities of the cobalt-(μ-oxo) moiety in **2**. Unfortunately, the structural data (despite several data collections) could not be fully refined to a satisfactory residual although there is no doubt of the atom connectivity. In contrast to the behavior of **2**, **1** is stable at room temperature. The pentane solution of **1** can be stirred at room temperature under nitrogen for 2 weeks without visible change.

Structures. The solid-state structures of **1** (Figure 1), **2** (Figure 2), and **3** (Figure 3) were determined by X-ray

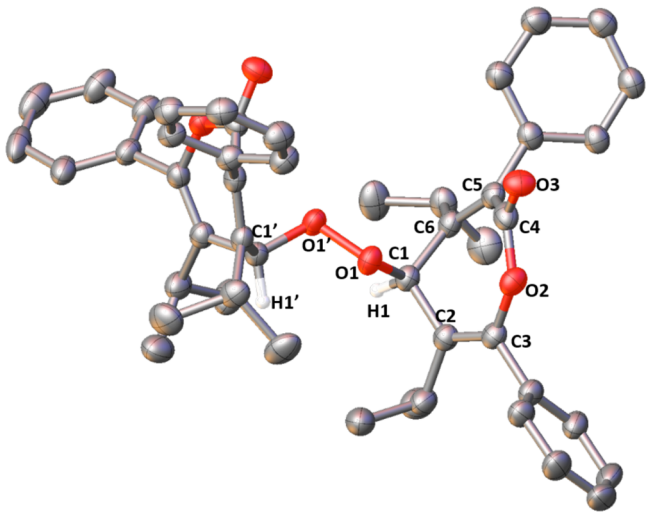

Figure 3. Solid-state molecular structure of **3** (H atoms except H(1) and H(1′) and isopropyl groups on the flanking rings are not shown, thermal ellipsoids are shown at 50% probability). Selected bond lengths (Å): O(1)−O(1′) 1.4956(18), O(1)−C(1) 1.461(2), C(1)−C(2) 1.519(2), C(2)−C(3) 1.336(2), C(3)−O(2) 1.392(2), O(2)−C(4) 1.403(2), C(4)−O(3) 1.210(2), C(4)−C(5) 1.463(3), C(5)−C(6) 1.340(3), C(6)−C(1) 1.520(3).

crystallography.[40] Selected bond distances and angles for **1** and **2** are given in the respective figure captions. Despite their similar stoichiometries, **1** and **2** display distinct structural features. In complex **1**, each iron(III) cation is formally coordinated by two bridging oxygens and an oxygen from a terminal aryloxide ligand, Ar^{iPr_8}O, but the sums of the three O−Fe−O angles at each iron are Fe(1), 334.96°, and Fe(2), 332.89°, indicating pyramidal coordination in the FeO_3 moieties. Consistent with the pyramidalization of the FeO_3 moiety, the metal ions display relatively close interaction with a *meta*-carbon of a flanking aryl ring (Fe(1)···C(14) 2.457(3) Å, Fe(2)···C(56) 2.427(3) Å). Thus, the coordination environment of the iron(III) cations may be considered to have a very distorted tetrahedral geometry.

DOI: 10.1021/acs.inorgchem.5b00930
Inorg. Chem. 2015, 54, 8914−8922

Apart from the previously unknown {ArylOFe(μ-O)}$_2$ stoichiometry, a noteworthy feature of the structure of **1** is the planar Fe$_2$(μ-O)$_2$ diamond core structure, which contains a short Fe···Fe distance of 2.4817(7) Å. This value is shorter than the 2.52 Å interatomic distance in iron metal[49] and approaches the value of 2.46 Å observed[15] in the MMO intermediate *Q*, suggesting a possible Fe−Fe bonding interaction in **1**. Only one Fe$_2$(μ-O)$_2$ complex has a comparable Fe···Fe distance: the complex [{(*N*,*N*′-Pipiso)Fe(μ-O)}$_2$] (Pipiso$^-$ = [(DippN)$_2$C-(*cis*-2,6-Me$_2$NC$_5$H$_8$)]$^-$, Dipp = C$_6$H$_3$Pr$^i_2$-2,6) which features four-coordinate iron ions and has an Fe···Fe separation of 2.475(1) Å.[22] Short Fe···Fe distances have also been seen in the iron-imide clusters Fe$_2$(μ-N^{t}Bu)$_2$Cl$_2$(NH$_2$^{t}Bu)$_2$, Fe$_2$(μ-N^{t}Bu)$_2$Cl$_2$(DMAP)$_2$, and Fe$_2$(μ-N^{t}Bu)$_2$Cl$_2$(PEt$_3$)$_2$, which have Fe$_2$(μ-N^{t}Bu)$_2$ cores.[50] The Fe···Fe distance in **1** is more than 0.2 Å shorter than those in other reported Fe$_2$(μ-O)$_2$ species, such as {Fe$_2$(μ-O)$_2$(6-Me$_3$-TPA)$_2$}{(ClO$_4$)$_2$} (2.716(2) Å),[19] {Fe$_2$(μ-O)$_2$(5-Et$_3$-TPA)$_2$}{(ClO$_4$)$_3$} (2.683(1) Å),[20] and {Fe$_2$(μ-O)$_2$(TAPA)$_2$}{(ClO$_4$)$_2$} (2.706(3) Å).[21] Within the Fe$_2$(μ-O)$_2$ core the Fe−O distances (Fe(1)−O(3) 1.818(3) Å, Fe(1)−O(4) 1.824(2) Å, Fe(2)−O(3) 1.829(2) Å, Fe(2)−O(4) 1.816(2) Å) are relatively uniform and shorter than the terminal Fe−O bond lengths (1.864(2) and 1.874(2) Å) to the aryloxide ligands. In contrast, the tris(2-pyridylmethyl)amine (TPA) model compounds all display more asymmetric bridging bonding modes, with variation in the Fe−O bond lengths of 0.05−0.07 Å,[19−21] probably because the ligands in those models are not as symmetric as the terphenyl ligand and are also multidentate in character. The reason that **1** has such a short iron−iron distance is probably similar to the Fe$_2$(μ-N^{t}Bu)$_2$ cases:[50] the combination of the short Fe−O bonds, the very symmetric diamond core structure, the interatomic repulsions between oxygen atoms in the diamond core, and the pseudotetrahedral coordination for iron which favors a wide O−Fe−O angle. Thus, in the rhombic core structure the Fe··· Fe axis is compressed.

In agreement with the short Fe···Fe separation and symmetric bonding mode, the acute Fe−O−Fe bridging angles (85.99(11)° and 85.76(11)°) are the smallest that have been reported in Fe$_2$(μ-O)$_2$ species.[19−22] The terminal Fe(1)−O(1)−C(1) (127.2(2)°) and Fe(2)−O(2)−C(43) angles (126.4(2)°) are considerably smaller than the terminal Fe−O−C angles in three-coordinate {Fe(OMes*)$_2$}$_2$ (161.8(6)°, Mes* = 2,4,6-^{t}Bu$_3$C$_6$H$_2$)[51] and Fe$_2$(μ-Mes)$_2$(Mes)(OMes*) (175.6(5)°, Mes = 2,4,6-Me$_3$C$_6$H$_2$),[52] possibly as a result of the secondary Fe···C interactions which attract the π-electron density found on a flanking aryl ring and result in a decrease in the Fe−O−C angles. The terminal Fe−O distances in **1** (1.864(3) and 1.874(3) Å) are somewhat longer than those in {Fe(OMes*)$_2$}$_2$ (1.822(5) Å)[51] and Fe$_2$(μ-Mes)$_2$(Mes)-(OMes*) (1.783(5) Å),[52] an increase which may be attributed to the large size of the terphenyl substituent[53−56] and the higher effective coordination number of the iron(III) ions in **1**. The plane of the central Fe$_2$(μ-O)$_2$ unit is almost perpendicular to the central phenyl rings of the ligands with the large torsion angles of 74.53(10)° and 77.55(10)°.

The structure of **2** (Figure 2) features similar connectivity to that of **1**, but with two pseudo-square-planar coordinated cobalt(III) ions bridged by two oxo groups and an oxygen inserted into each of the Co−C bonds. Apart from the low formal metal ion coordination number of three, which is extremely rare for cobalt(III),[26,27,57,58] the most striking feature of the structure is the Co(1)···Co(2) distance (2.7209(4) Å) which is ca. 0.24 Å longer than the corresponding Fe···Fe distance in **1** despite the smaller size of cobalt(III) relative to iron(III). This is probably because the quasi-square-planar coordination geometry for cobalt(III) favors narrower O−Co−O angles than the quasitetrahedral coordination geometry for iron(III). Thus, the Co−O−Co angles are opened, and the Co···Co distance is increased. The Co···Co distance is ca. 0.26 Å longer than that predicted for a cobalt−cobalt single bond (2.46 Å),[59] suggesting little or no Co−Co bonding interaction in **2**. This Co···Co separation is comparable to those found[23−27] in the structures of other complexes containing a Co(III)$_2$(μ-O)$_2$ core and higher metal coordination numbers. In particular, it almost matches the corresponding distances in [(HC{C(Me)NC$_6$H$_3$-2,6-Me$_2$}$_2$)Co]$_2$(μ-O)$_2$ (2.716(4) Å)[26] and (Tp$^{Me}_3$Co)$_2$(μ-O)$_2$ (2.728(2) Å, Tp$^{Me}_3$ = hydrotris(3,4,5-trimethyl-1-pyrazolyl)borate).[23] The distance between the two bridging oxygens (O(2)···O(3) 2.283(2) Å) is long enough to exclude the existence of any peroxo or superoxo character for the compound. Another feature of the solid-state structure of **2** is the short cobalt-oxo distances (1.7690(14)−1.7831(14) Å) within the Co$_2$(μ-O)$_2$ core. These values are close to but shorter than the range of cobalt-oxo bond distances reported in related Co(III)$_2$(μ-O)$_2$ complexes (1.783(4)−1.832(5) Å)[23−27] that feature four- or five-coordinate cobalt(III) ions. This is probably a result of the lower formal coordination number of three for the metal. Similar to **1**, the terminal Co(1)−O(1) (1.8287(13) Å) and Co(2)−O(4) (1.8299(13) Å) bonds in **2** are somewhat longer than the bridging Co−O distances and are slightly shorter than the 1.836(2)−1.853(2) Å range of distances seen for terminal Co−O bonds in monomeric Co(II) aryloxides.[60] As was observed in **1**, the Co(1)−O(1)−C(1) (120.48(12)°) and Co(2)−O(4)−C(43) (120.51(12)°) angles are narrower than the Co−O−C angles in the structurally related dimeric Co(II) alkoxides [Co{OC(C$_6$H$_{11}$)$_3$}$_2$]$_2$ (Co(1)−O(1)−C(1) 145.2(4)°, Co(2)−O(2)−C(20) 158.1(5)°)[61] and possibly result from secondary interactions.

The interligand angles at the cobalt(III) ions in **2** (range ca. 80−189°) are much greater than those in **1** such that the geometries of the CoO$_3$ units may be considered to be approximately T-shaped with a planar metal coordination ($\sum$° Co(1) = 360.50°, Co(2) = 360.47°). In addition to bonding to three oxygens, each cobalt(III) cation has a short secondary interaction with the *ipso* carbon of one of the flanking aryl rings of the terphenyl ligand (Co(1)···C(13) 2.2867(18) Å, Co(2)··· C(55) 2.2672(18) Å). Thus, both cobalt(III) cations may also be considered as effectively four-coordinate, with a distorted square planar coordination geometry (including the *ipso* carbons) as is indicated by the sum of the CoO$_3$C(*ipso*) interligand angles of 360.04° and 359.77° at Co(1) and Co(2), respectively. Furthermore, the Co$_2$(μ-O)$_2$ core also has a planar structure, so that the two cobalt(III) cations, four oxygen atoms, and two carbon atoms are all essentially coplanar. In contrast to the structure of **1**, the Co$_2$(μ-O)$_2$ ring in **2** is almost coplanar (torsion angles = 2.21(7)° and 2.90(7)°) with the central phenyl rings of the ligands.

In the structure of the peroxide **3** (Figure 3), the O(1)−O(1′) distance (1.4956(18) Å) is slightly longer than the O−O distance in hydrogen peroxide (1.475 Å)[62] but very close to the O−O bond length in bis(1-morpholinocyclohex-1-yl)peroxide 1.497(3) Å,[63] and 4,4′-dioxybis(2-(2-*t*-butylphenyl)-4,5-diphenyl-4*H*-imidazole) 1.496(2) Å.[64] The bond lengths of C(2)−C(3) (1.336(2) Å), C(5)−C(6) (1.340(3) Å), and C(4)−O(3) (1.210(2) Å) lie well in the range of carbon−carbon (∼1.34 Å)

DOI: 10.1021/acs.inorgchem.5b00930
Inorg. Chem. 2015, 54, 8914−8922

or carbon−oxygen (~1.22 Å) double bond lengths.[62] Specifically, those bond lengths are similar to the corresponding bond lengths (carbon−carbon double bond lengths of 1.330(3) and 1.331(3) Å and carbon−oxygen double bond lengths of 1.196(2) Å) in the dihydro-oxepine 2-(3,6-di-*t*-butyl-7-oxo-4-(4,4,5,5-tetramethyl-4,5-dihydro-1*H*-imidazol-1-yloxy)-4*H*-oxepin-2-yl)-4,4,5,5-tetramethyl-4,5-dihydro-1*H*-imidazol-3-oxide-1-oxyl.[65] The C(4)−O(3) double bond moiety and O(2) (oxygen atom in the seven membered ring) are modeled with a positional disorder of the enoate moiety. The major occupancy site (82%) is illustrated in Figure 3.

Magnetic and Mössbauer Spectral Properties. The magnetic properties of both **1** and **2** were investigated by SQUID magnetometry (solid state) and the Evans method (solution state). The temperature dependence of $\chi_M T$ for **1** in the solid state with its fit is shown in Figure 4; the decrease in

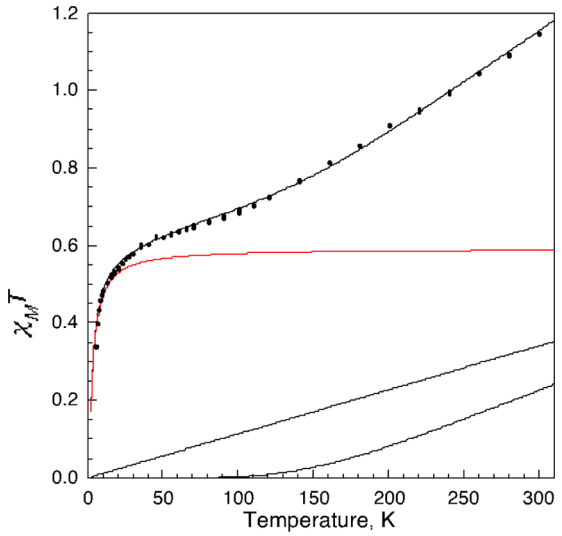

Figure 4. Temperature dependence of $\chi_M T$ obtained at 0.01 T for **1** and the best fit between 5 and 300 K, black line, obtained for $S_1 = S_2 = {}^5/_2$, $g = 2$, with $J = -240(20)$ cm^{-1} for the Fe(1)···Fe(2) magnetic exchange, lowest black curve, and an average $N\alpha = 0.0011(2)$ emu/mol or 0.000 55(20) emu/mol for iron(III), lowest straight black line. The red line corresponds to 7.0(1) wt % of an iron(III) dimeric impurity with $S_1 = S_2 = {}^5/_2$, $g = 2$, and $J = -0.26(2)$ cm^{-1}.

$\chi_M T$ is the result of antiferromagnetic exchange between the two $S = {}^5/_2$ pseudotetrahedral iron(III) cations found in **1**, which are separated by a short Fe(1)···Fe(2) distance of 2.4817(7) Å and have two through-bond distances of 3.641(6) and 3.634(6) Å. These structural parameters are well-suited for both antiferromagnetic direct exchange and/or superexchange between the two iron(III) ions. The temperature dependence of $\chi_M T$ of **1** has been fit between 5 and 300 K with the $H = -2JS_1 \cdot S_2$ Hamiltonian, and the result is shown by the solid curves in Figure 4. The magnetic exchange coupling constant, $J = -240(20)$ cm^{-1}, is more negative than would typically be expected[66] for antiferromagnetic superexchange through the two ca. 86° bridging angles at O(3) and O(4). Thus, the very negative *J*-value may indicate the importance of direct exchange between the Fe(1)···Fe(2) cations that are separated by only 2.4817(7) Å, a separation which may yield a substantial Fe−Fe bonding interaction that leads to the observed strong antiferromagnetic exchange interaction. Indeed, a rather large value of $J = -145$ cm^{-1}, based on magnetic data obtained between ca. 120 and 300 K, has been reported[22] for a pseudotetrahedral iron(III) dioxo-bridged dimeric complex that exhibits a similar short Fe···Fe distance of 2.475(1) Å and similar Fe−O−Fe bridging angles. The less negative *J*-value in the latter case may be the result of the very different fitting approach, the restricted temperature range, and the presence of ca. 20% of a monomeric iron(III) paramagnetic impurity. As expected, the exchange coupling of $J = -240$ cm^{-1} observed for **1** is far more negative than the $J = -33.5$ cm^{-1} reported[19] for a pseodooctahedral iron(III) dioxo-bridged dimeric complex that exhibits an Fe···Fe distance of 2.714(2) Å. In d_6-benzene solution, the magnetic moment of **1** is 3.26 μ_B per dimer, which is close to the magnetic moment determined in the solid state (3.08 μ_B). As will be discussed below, these magnetic moments result from the presence of a small amount of high-spin iron(III) impurity in the sample under study.

An X-band EPR measurement was attempted, but **1** is EPR silent, probably because of the large negative magnetic exchange coupling constant between the iron cations.

The Mössbauer spectrum of **1** has been measured at 80 K and is shown with its fit in Figure 5. Because **1** contains two

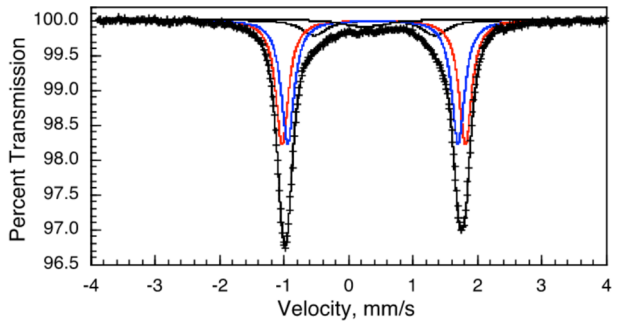

Figure 5. Mössbauer spectrum of **1** at 80 K. The red and blue doublets correspond to the two crystallographically distinct iron(III) sites in **1**. The two less intense doublets correspond to high-spin iron(III) impurities.

crystallographically distinct iron(III) cations with slightly different hyperfine parameters, the observed spectrum is somewhat asymmetric. As a consequence, the spectrum has been fit with two symmetric quadrupole doublets, the red and blue components in Figure 5, each with the same relative area of 42.5(1)% and a line width of $\Gamma = 0.228(2)$ mm/s. The corresponding hyperfine parameters for the first doublet are $\delta = 0.378(1)$ mm/s for the isomer shift and $\Delta E_Q = 2.643(2)$ mm/s for the quadrupole splitting; the parameters for the second doublet are $\delta = 0.391(1)$ mm/s and $\Delta E_Q = 2.840(2)$ mm/s. The relatively large quadrupole splittings result because of the highly distorted quasitetrahedral iron(III) coordination environments of three oxygens and one carbon and/or the strong Fe−Fe interaction resulting from the short Fe···Fe distance. This highly distorted iron(III) environment in **1** leads to a much larger quadrupole splitting than the 0.77 mm/s observed[22] in an approximately tetrahedral complex and the 1.93 mm/s observed[19] in a pseudooctahedral complex. Further, the isomer shift of **1** is typical of a high-spin iron(III) cation in a pseudotetrahedral coordination environment[22,67] and is also similar to the isomer shifts observed for some comparable iron(III) complexes with trigonal coordination environments,[68,69] but, as expected, is somewhat lower than that

DOI: 10.1021/acs.inorgchem.5b00930
Inorg. Chem. 2015, 54, 8914−8922

observed[19] in a distorted octahedrally coordinated oxo-bridged iron(III) dimer.

Because of the extreme sensitivity of **1** to air and moisture, the spectrum also exhibits the presence of small amounts of iron(III) impurities that correspond to the spectral components shown in black in Figure 5. The more intense of these components has δ = 0.404(7) mm/s, ΔE_Q = 1.88(2) mm/s, Γ = 0.48(4) mm/s, and a relative area of 11(1)%; the less intense of these components has δ = 0.26(2) mm/s, ΔE_Q = 0.35(4) mm/s, Γ = 0.5(1) mm/s, and a relative area of 3.8(5)%. These two components, and especially the more intense one, probably yield the impurity noted above in the magnetic properties of **1**, shown in red in Figure 4.

Compound **2** exhibits very different magnetic properties from **1**, presumably because of the different coordination environments about the cobalt(III) and iron(III) ions. The temperature dependence of $\chi_M T$ for **2** with its fit is shown in Figure 6, where S = 1 was used as expected for a pseudo-square-planar cobalt(III) ion. The fit reveals a ferromagnetic exchange coupling with a coupling constant of J = +7.7(2) cm^{-1}, a very weak long-range antiferromagnetic coupling of zJ = −0.069(4) cm^{-1}, and a temperature independent paramagnetic susceptibility, $N\alpha$ = 0.00101(2) emu/mol, parameters which are reasonable for **2**. The magnetic moment was determined to be 3.96 μ_B per dimer in solution (C_6D_6, Evans' method), which is close to the magnetic moment determined in the solid state (4.29 μ_B). The X-band EPR measurement of **2** did not show any cobalt(III) characteristic signal (Figure S2), probably because the zero-field splitting value range for square planar cobalt(III) complexes is usually between 30 and 40 cm^{-1},[70] which is too large to permit an X-band EPR measurement. Instead, a very narrow signal showed up at $g \approx 2$, possibly from radical intermediates during the decomposition of **2**.

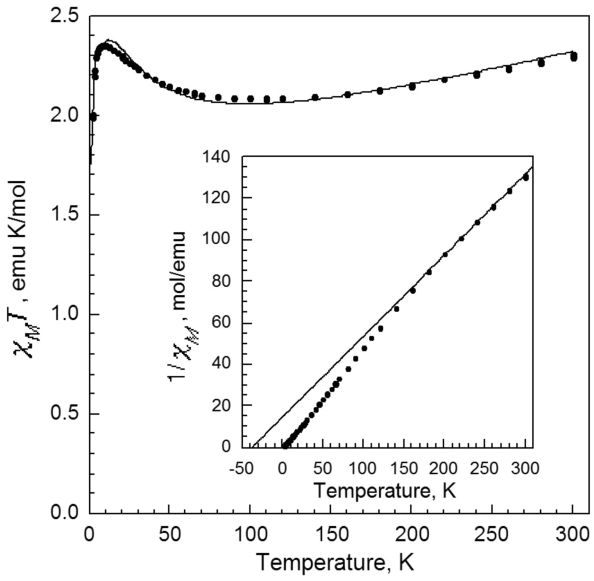

Figure 6. Temperature dependence of $\chi_M T$ obtained at 0.01 T for **2** and the best fit between 5 and 300 K, black line, obtained with S = 1, g = 1.809(4), intramolecular ferromagnetic exchange coupling J = +7.7(2) cm^{-1}, weak long-range antiferromagnetic coupling zJ = −0.069(4) cm^{-1}, and $N\alpha$ = 0.00101(2) emu/mol. Inset shows the temperature dependence of $1/\chi_M$ fit between 150 and 300 K with the Curie−Weiss law.

Density Functional Calculations. DFT full molecule calculations for **1** were carried out at the M06-2x level, by using the 6-311+G(d) basis set for the iron cations, the 6-31G(d) basis set for oxygen, and the 6-31G basis set for C and H atoms. The DFT optimized structure of **1** is shown in Figure S3, and selected calculated and experimental bond lengths and angles are listed in Table S2. The fully optimized calculated structural distances are mostly in good agreement with the experimental distances, although there are deviations in the metal(III)···metal(III) and the secondary metal(III)···carbon distances that are larger than those observed for the other parameters, as is indicated by Fe(1)···Fe(2) = 2.639 Å (calculated) versus 2.4817(7) Å (experimental), and Fe(1)···C(14) = 2.655 Å (calculated) versus 2.457(3) Å (experimental) distances. We have tried with different functionals and spin states to optimize the structure. For **1**, the total S = 5 spin state and its $2S + 1$ = 11 undecet spin state yield the most stable structure and the M06-2x functional gives the closest results to the experimental data. Details of DFT calculation are included in Figures S3−S6 and Tables S2−S5 in the Supporting Information.

Electrochemistry. Cyclic voltammetry was performed on **1** and **2**. The two complexes showed different redox properties. Complex **1** in THF solution showed two irreversible reductions at E_p = −0.680 V (vs Fc/Fc$^+$, Fc = ferrocene) and E_p = −1.358 V (vs Fc/Fc$^+$) and one reversible i_{pa}/i_{pc} = 0.79 reduction event at $E_{1/2}$ = −0.833 V (vs Fc/Fc$^+$). In contrast, the cyclic voltammetry of **2** revealed two irreversible reduction events at E_p = −0.839 V (vs Fc/Fc$^+$) and E_p = −1.428 V (vs Fc/Fc$^+$). Unlike $[Fe^{III}Fe^{IV}(\mu\text{-}O)_2(L)_2](ClO_4)_3$ (L = tris(4-methoxy-3,5-dimethylpyridyl-2-methyl)amine), which can be oxidized electrochemically by one electron,[71] further oxidation event for either **1** or **2** was not observed.

CONCLUSIONS

The unusual bis(μ-oxo) dimeric complexes $\{Ar^{iPr_8}OM(\mu\text{-}O)\}_2$ (M = Fe (**1**), Co (**2**)) have been synthesized and structurally characterized. Their solid-state structures contain an $M_2(\mu\text{-}O)_2$ core with a significantly shorter Fe···Fe distance in **1** than the corresponding Co···Co distance in **2**. The Fe−Fe distance is similar to that in the diamond core structure proposed for methane monooxygenase intermediate Q. The stability of the cobalt species **2** is much lower than that of its iron counterpart **1**. Complexes **1** and **2** display very different magnetic properties due to their unusual structural differences. The density functional computed structure for **1** mostly showed good agreement with the crystallographic data, and the major absorption in the UV−vis spectrum of **1** results from ligand to metal(III) cation charge transfer. The cobalt complex **2** decomposes at room temperature within 3 days to afford **3**. An unexpected C−C bond oxidation occurred, and a peroxy moiety was formed. The structure of **3** is closely related to that of a key intermediate proposed for the oxidation of benzene, which is a very important process for fuel autoignition and atmospheric chemistry.

Further exploration of the reactivity of **1** and **2** and their application as C−H oxidation and aryl oxidation catalysts are underway.

ASSOCIATED CONTENT

Supporting Information

The Supporting Information is available free of charge on the ACS Publications website at DOI: 10.1021/acs.inorgchem.5b00930.

DOI: 10.1021/acs.inorgchem.5b00930
Inorg. Chem. 2015, 54, 8914−8922

X-ray crystallographic refinement data for **1**, **2**, and **3**; EPR X-band spectra of **2**; details of DFT calculations on **1** and **2**; cyclic voltammograms for **1** and **2** (PDF)
Crytallographic details for **1**, **2**, and **3** (CIF)
Method for optimization (TXT)

AUTHOR INFORMATION

Corresponding Authors

*E-mail: glong@mst.edu.
*E-mail: nagase@ims.ac.jp.
*E-mail: pppower@ucdavis.edu.

Present Address

[‖]MABE Department, University of Tennessee Space Institute, Tullahoma, Tennessee 37388, United States.

Notes

The authors declare no competing financial interest.

ACKNOWLEDGMENTS

We are grateful to the U.S. National Science Foundation (CHE-1263760) for financial support. National Institutes of Health is acknowledged for the Mössbauer equipment with Grant 1S10RR023656-01A1. We thank Dr. Peter Klavins for the help with SQUID measurements. P.Z. thanks Emily Thompson and Prof. Louise Berben for cyclic voltammetry measurements and Ryan Wall, Dr. Troy Stich, and Prof. R. David Britt for the EPR measurements.

REFERENCES

(1) Shilov, A. E.; Shul'pin, G. B. *Chem. Rev.* **1997**, *97*, 2879.
(2) Stahl, S. S. *Angew. Chem., Int. Ed.* **2004**, *43*, 3400.
(3) Dick, A. R.; Sanford, M. S. *Tetrahedron* **2006**, *62*, 2439.
(4) Punniyamurthy, T.; Velusamy, S.; Iqbal, J. *Chem. Rev.* **2005**, *105*, 2329.
(5) Que, L.; Tolman, W. B. *Nature* **2008**, *455*, 333.
(6) Gunay, A.; Theopold, K. H. *Chem. Rev.* **2010**, *110*, 1060.
(7) Yin, G. *Coord. Chem. Rev.* **2010**, *254*, 1826.
(8) Borovik, A. S. *Chem. Soc. Rev.* **2011**, *40*, 1870.
(9) Ray, K.; Pfaff, F. F.; Wang, B.; Nam, W. *J. Am. Chem. Soc.* **2014**, *136*, 13942.
(10) Lee, S. K.; Nesheim, J. C.; Lipscomb, J. D. *J. Biol. Chem.* **1993**, *268*, 21569.
(11) Liu, K. E.; Valentine, A. M.; Wang, D.; Huynh, B. H.; Edmondson, D. E.; Salifoglou, A.; Lippard, S. J. *J. Am. Chem. Soc.* **1995**, *117*, 10174.
(12) Nesheim, J. C.; Lipscomb, J. D. *Biochemistry* **1996**, *35*, 10240.
(13) Tinberg, C. E.; Lippard, S. J. *Biochemistry* **2010**, *49*, 7902.
(14) Tinberg, C. E.; Lippard, S. J. *Acc. Chem. Res.* **2011**, *44*, 280.
(15) Shu, L.; Nesheim, J. C.; Kauffmann, K.; Münck, E.; Lipscomb, J. D.; Que, L. *Science* **1997**, *275*, 515.
(16) Banerjee, R.; Proshlyakov, Y.; Lipscomb, J. D.; Proshlyakov, D. A. *Nature* **2015**, *518*, 431.
(17) Que, J. L.; Tolman, W. B. *Angew. Chem., Int. Ed.* **2002**, *41*, 1114.
(18) Friedle, S.; Reisner, E.; Lippard, S. J. *Chem. Soc. Rev.* **2010**, *39*, 2768.
(19) Zang, Y.; Dong, Y.; Que, L.; Kauffmann, K.; Muenck, E. *J. Am. Chem. Soc.* **1995**, *117*, 1169.
(20) Hsu, H.-F.; Dong, Y.; Shu, L.; Young, V. G.; Que, L. *J. Am. Chem. Soc.* **1999**, *121*, 5230.
(21) Honda, Y.; Arii, H.; Okumura, T.; Wada, A.; Funahashi, Y.; Ozawa, T.; Jitsukawa, K.; Masuda, H. *Bull. Chem. Soc. Jpn.* **2007**, *80*, 1288.
(22) Fohlmeister, L.; Vignesh, K. R.; Winter, F.; Moubaraki, B.; Rajaraman, G.; Pöttgen, R.; Murray, K. S.; Jones, C. *Dalton Trans.* **2015**, *44*, 1700.
(23) Hikichi, S.; Yoshizawa, M.; Sasakura, Y.; Akita, M.; Moro-oka, Y. *J. Am. Chem. Soc.* **1998**, *120*, 10567.
(24) Hikichi, S.; Yoshizawa, M.; Sasakura, Y.; Komatsuzaki, H.; Moro-oka, Y.; Akita, M. *Chem. - Eur. J.* **2001**, *7*, 5011.
(25) Larsen, P. L.; Parolin, T. J.; Powell, D. R.; Hendrich, M. P.; Borovik, A. S. *Angew. Chem., Int. Ed.* **2003**, *42*, 85.
(26) Dai, X.; Kapoor, P.; Warren, T. H. *J. Am. Chem. Soc.* **2004**, *126*, 4798.
(27) Jones, C.; Schulten, C.; Rose, R. P.; Stasch, A.; Aldridge, S.; Woodul, W. D.; Murray, K. S.; Moubaraki, B.; Brynda, M.; La Macchia, G.; Gagliardi, L. *Angew. Chem., Int. Ed.* **2009**, *48*, 7406.
(28) Ni, C.; Ellis, B. D.; Fettinger, J. C.; Long, G. J.; Power, P. P. *Chem. Commun.* **2008**, 1014.
(29) Lei, H.; Ellis, B. D.; Ni, C.; Grandjean, F.; Long, G. J.; Power, P. P. *Inorg. Chem.* **2008**, *47*, 10205.
(30) Ni, C.; Fettinger, J. C.; Long, G. J.; Brynda, M.; Power, P. P. *Chem. Commun.* **2008**, 6045.
(31) Kovaleva, E. G.; Lipscomb, J. D. *Nat. Chem. Biol.* **2008**, *4*, 186.
(32) Siegbahn, P. E. M.; Haeffner, F. *J. Am. Chem. Soc.* **2004**, *126*, 8919.
(33) Kovaleva, E. G.; Lipscomb, J. D. *Science* **2007**, *316*, 453.
(34) Zádor, J.; Taatjes, C. A.; Fernandes, R. X. *Prog. Energy Combust. Sci.* **2011**, *37*, 371.
(35) Schuetzle, D.; Siegl, W. O.; Jensen, T. E.; Dearth, M. A.; Kaiser, E. W.; Gorse, R.; Kreucher, W.; Kulik, E. *Environ. Health Perspect.* **1994**, *102*, 3.
(36) Yamada, E.; Hosokawa, Y.; Furuya, Y.; Matsushita, K.; Fuse, Y. *Anal. Sci.* **2004**, *20*, 107.
(37) Savee, J. D.; Papajak, E.; Rotavera, B.; Huang, H.; Eskola, A. J.; Welz, O.; Sheps, L.; Taatjes, C. A.; Zádor, J.; Osborn, D. L. *Science* **2015**, *347*, 643.
(38) Bain, G. A.; Berry, J. F. *J. Chem. Educ.* **2008**, *85*, 532.
(39) *SADABS, Version 8.27b*; Bruker AXS Inc.: Madison, WI, 2008.
(40) Sheldrick, G. M. *SHELXTL, Version 6.1*; Bruker AXS Inc.: Madison, WI, 2002.
(41) Frisch, M. J.; Trucks, G. W.; Schlegel, H. B.; Scuseria, G. E.; Robb, M. A.; Cheeseman, J. R.; Scalmani, G.; Barone, V.; Mennucci, B.; Petersson, G. A.; Nakatsuji, H.; Caricato, M.; Li, X.; Hratchian, H. P.; Izmaylov, A. F.; Bloino, J.; Zheng, G.; Sonnenberg, J. L.; Hada, M.; Ehara, M.; Toyota, K.; Fukuda, R.; Hasegawa, J.; Ishida, M.; Nakajima, T.; Honda, Y.; Kitao, O.; Nakai, H.; Vreven, T.; Montomgery, J. M., Jr.; Peralta, J. E.; Ogliaro, F.; Bearpark, M.; Heyd, J. J.; Brothers, E.; Kudin, K. N.; Staroverov, V. N.; Kobayashi, R.; Normand, J.; Raghavachari, K.; Rendell, A.; Burant, J. C.; Iyengar, S. S.; Tomasi, J.; Cossi, M.; Rega, N.; Millam, J. M.; Klene, M.; Knox, J. E.; Cross, J. B.; Bakken, V.; Adamo, C.; Jaramillo, J.; Gomperts, R.; Stratmann, R. E.; Yazyev, O.; Austin, A. J.; Cammi, R.; Pomelli, C.; Ochterski, J. W.; Martin, R. L.; Morokuma, K.; Zakrzewski, V. G.; Voth, G. A.; Salvador, P.; Dannenberg, J. J.; Dapprich, S.; Daniels, A. D.; Farkas, O.; Foresman, J. B.; Ortiz, J. V.; Cioslowski, J.; Fox, D. J. *Gaussian 09, Revision A.01*; Gaussian Inc.: Wallingford, CT, 2009.
(42) Yanai, T.; Tew, D. P.; Handy, N. C. *Chem. Phys. Lett.* **2004**, *393*, 51.
(43) Ni, C.; Power, P. P. *Chem. Commun.* **2009**, 5543.
(44) Prince, B. M.; Cundari, T. R.; Tymczak, C. J. *J. Phys. Chem. A* **2014**, *118*, 11056.
(45) Dai, F.; Yap, G. P. A.; Theopold, K. H. *J. Am. Chem. Soc.* **2013**, *135*, 16774.
(46) Boaz, N. C.; Bell, S. R.; Groves, J. T. *J. Am. Chem. Soc.* **2015**, *137*, 2875.
(47) Merle, J. K.; Hadad, C. M. *J. Phys. Chem. A* **2004**, *108*, 8419.
(48) Kroner, S. M.; DeMatteo, M. P.; Hadad, C. M.; Carpenter, B. K. *J. Am. Chem. Soc.* **2005**, *127*, 7466.
(49) Wells, A. F. *Structural Inorganic Chemistry*; Oxford: New York, 1984.
(50) Duncan, J. S.; Zdilla, M. J.; Lee, S. C. *Inorg. Chem.* **2007**, *46*, 1071.
(51) Bartlett, R. A.; Ellison, J. J.; Power, P. P.; Shoner, S. C. *Inorg. Chem.* **1991**, *30*, 2888.

DOI: 10.1021/acs.inorgchem.5b00930
Inorg. Chem. 2015, 54, 8914−8922

(52) Müller, H.; Seidel, W.; Görls, H. *Z. Anorg. Allg. Chem.* **1996**, *622*, 1968.
(53) Twamley, B.; Haubrich, S. T.; Power, P. P. In *Advances in Organometallic Chemistry*; West, R., Hill, A. F., Eds.; Academic Press: New York, 1999; Vol. *44*, p 1.
(54) Clyburne, J. A. C.; McMullen, N. *Coord. Chem. Rev.* **2000**, *210*, 73.
(55) Power, P. P. *J. Organomet. Chem.* **2004**, *689*, 3904.
(56) Ni, C.; Power, P. P. In *Metal-Metal Bonding*; Parkin, G., Ed.; Springer: Berlin, 2010; Vol. *136*, p 59.
(57) Ellison, J. J.; Power, P. P.; Shoner, S. C. *J. Am. Chem. Soc.* **1989**, *111*, 8044.
(58) King, E. R.; Sazama, G. T.; Betley, T. A. *J. Am. Chem. Soc.* **2012**, *134*, 17858.
(59) Pauling, L. *Proc. Natl. Acad. Sci. U. S. A.* **1976**, *73*, 4290.
(60) Bryan, A. M.; Long, G. J.; Grandjean, F.; Power, P. P. *Inorg. Chem.* **2014**, *53*, 2692.
(61) Sigel, G. A.; Bartlett, R. A.; Decker, D.; Olmstead, M. M.; Power, P. P. *Inorg. Chem.* **1987**, *26*, 1773.
(62) Dewar, M. J. S.; Thiel, W. *J. Am. Chem. Soc.* **1977**, *99*, 4899.
(63) Starostin, E. K.; Khrustalev, V. N.; Antipin, M. Y.; Lalov, A. V. *Mendeleev Commun.* **2009**, *19*, 334.
(64) Edkins, R. M.; Probert, M. R.; Fucke, K.; Robertson, C. M.; Howard, J. A. K.; Beeby, A. *Phys. Chem. Chem. Phys.* **2013**, *15*, 7848.
(65) Tretyakov, E. V.; Tolstikov, S. E.; Romanenko, G. V.; Bogomyakov, A. S.; Cherkasov, V. K.; Stass, D. V.; Ovcharenko, V. I. *Russ. Chem. Bull.* **2011**, *60*, 2325.
(66) Gingsberg, A. P. *Inorg. Chim. Acta, Rev.* **1971**, *5*, 45.
(67) Greenwood, N. N.; Gibb, T. C. *Mössbauer Spectroscopy*; Chapman and Hall: London, 1971.
(68) Fitzsimmons, B. W.; Johnson, C. E. *Chem. Phys. Lett.* **1974**, *24*, 422.
(69) Eckert, N. A.; Vaddadi, S.; Stoian, S.; Lachicotte, R. J.; Cundari, T. R.; Holland, P. L. *Angew. Chem., Int. Ed.* **2006**, *45*, 6868.
(70) Ray, K.; Begum, A.; Weyhermüller, T.; Piligkos, S.; van Slageren, J.; Neese, F.; Wieghardt, K. *J. Am. Chem. Soc.* **2005**, *127*, 4403.
(71) Xue, G.; Wang, D.; De Hont, R.; Fiedler, A. T.; Shan, X.; Münck, E.; Que, L. *Proc. Natl. Acad. Sci. U. S. A.* **2007**, *104*, 20713.

DOI: 10.1021/acs.inorgchem.5b00930
Inorg. Chem. 2015, 54, 8914−8922